The University of
Nottingham

UNITED KINGDOM · CHINA · MALAYSIA

Rodriguez Del Pino, Bruno and Bamford, Steven P. and Aragón-Salamanca, Alfonso and Milvang-Jensen, Bo and Merrifield, Michael R. and Balcells, Marc (2014) Caught in the act: cluster 'k+a' galaxies as a link between spirals and S0s. Monthly Notices of the Royal Astronomical Society, 438 (2). pp. 1038-1050. ISSN 0035-8711

Access from the University of Nottingham repository:
http://eprints.nottingham.ac.uk/42056/1/stt2202.pdf

Copyright and reuse:

Caught in the act: cluster 'k+a' galaxies as a link between spirals and S0s

Bruno Rodríguez Del Pino,[1][★] Steven P. Bamford,[1] Alfonso Aragón-Salamanca,[1]
Bo Milvang-Jensen,[2] Michael R. Merrifield[1] and Marc Balcells[3,4,5]

[1]*School of Physics and Astronomy, The University of Nottingham, University Park, Nottingham NG7 2RD, UK*
[2]*Dark Cosmology Centre, Niels Bohr Institute, University of Copenhagen, Juliane Maries Vej 30, DK-2100 Copenhagen Ø, Denmark*
[3]*Isaac Newton Group of Telescopes, Apartado 321, E-38700 Santa Cruz de La Palma, Canary Islands, Spain*
[4]*Instituto de Astrofísica de Canarias, E-38200 La Laguna, Tenerife, Spain*
[5]*Department de Astrofísica, Universidad de La Laguna, E-38205 La Laguna, Tenerife, Spain*

ABSTRACT

We use integral field spectroscopy of 13 disc galaxies in the cluster AC114 at $z \sim 0.31$ in an attempt to disentangle the physical processes responsible for the transformation of spiral galaxies in clusters. Our sample is selected to display a dominant young stellar population, as indicated by strong Hδ absorption lines in their integrated spectra. Most of our galaxies lack the [O II]λ3727 emission line, and hence ongoing star formation. They therefore possess 'k+a' spectra, indicative of a recent truncation of star formation, possibly preceded by a starburst. Discy 'k+a' galaxies are a promising candidate for the intermediate stage of the transformation from star-forming spiral galaxies to passive S0s. Our observations allow us to study the spatial distributions and the kinematics of the different stellar populations within the galaxies. We used three different indicators to evaluate the presence of a young population: the equivalent width of Hδ, the luminosity-weighted fraction of A stars, and the fraction of the galaxy light attributable to simple stellar populations with ages between 0.5 and 1.5 Gyr. We find a mixture of behaviours, but are able to show that in most of the galaxies the last episode of star formation occurred in an extended disc, similar to preceding generations of stars, though somewhat more centrally concentrated. We thus exclude nuclear starbursts and violent gravitational interactions as causes of the star formation truncation. Gentler mechanisms, such as ram-pressure stripping or weak galaxy–galaxy interactions, appear to be responsible for ending star formation in these intermediate-redshift cluster disc galaxies.

Key words: galaxies: clusters: individual: AC114 – galaxies: evolution – galaxies: interactions.

1 INTRODUCTION

The properties of galaxies – such as morphology, colour, size and mass – vary according to the environment where they reside. In particular, galaxy morphologies have been shown to change with local projected density (e.g. Dressler 1980; Bamford et al. 2009), with late-type spiral and irregular galaxies showing more preference for regions with lower densities, while early-type S0 and elliptical galaxies are more abundant in denser regions. Although in a different time-scale, specific star formation rates, SSFR, are also affected by the environment (Balogh et al. 2004a; Vogt et al. 2004a) and has been shown to be the galaxy property most affected by the density of the environment (Kauffmann et al. 2004; Wolf et al. 2009). The concentration of the star formation in cluster disc galaxies is also found to be ∼25 per cent smaller than comparable galaxies in the field (Bamford, Milvang-Jensen & Aragón-Salamanca 2007).

There is also a change in the morphological make-up of the galaxy population with redshift, particularly in clusters. Spiral galaxies show high fractions in clusters at intermediate redshift ($z \sim 0.5$), where the fraction of S0s is low, but while the fraction of spirals decreases for local clusters, S0s become more dominant, being two to three times more abundant today than at intermediate redshift (Dressler et al. 1997). On the other hand, ellipticals do not show a substantial variation, comprising a significant fraction of cluster galaxies since at least $z \sim 1$ (Dressler et al. 1997; Fasano et al. 2000; Desai et al. 2007). Correspondingly, the fraction of star-forming blue galaxies in clusters has been shown to increase with redshift (Butcher & Oemler 1978, 1984; Margoniner et al. 2001), known as the Butcher–Oemler effect, and these have been found to comprise normal late-type spirals (Couch et al. 1994; Dressler et al. 1994).

All these different findings point to a transformation of galaxies from spiral into S0 within the cluster environment, as suggested in many studies (e.g. Larson, Tinsley & Caldwell 1980; Bekki, Couch

[★] E-mail: ppxbr@nottingham.ac.uk

& Shioya 2002; Shioya et al. 2002; Aragón-Salamanca, Bedregal & Merrifield 2006; Kormendy & Bender 2012). This transformation would start with blue, star-forming, spiral galaxies at intermediate redshift falling into regions of higher density such as groups and clusters, experiencing the loss of their gas and subsequent suppression of star formation, but retaining their discs, resulting in red, passive, S0 galaxies.

A variety of mechanisms have been suggested to be responsible for such transformations: interaction with the hot intracluster medium (ICM) via thermal evaporation (Nipoti & Binney 2007) and ram-pressure stripping (Gunn & Gott 1972; Abadi, Moore & Bower 1999; Bekki et al. 2002), interactions with the cluster tidal field (Larson et al. 1980), galaxy harassment (Moore et al. 1996) and minor mergers (Bekki et al. 2005; Eliche-Moral et al. 2012, 2013). All these processes may be expected to remove or disturb the gas contents of galaxies, while leaving the stellar distributions relatively unscathed. Major mergers can also trigger starbursts which may consume gas reservoirs and ultimately suppress star formation (Mihos & Hernquist 1996), although unless they are gas-rich (Hopkins et al. 2009), their stellar discs may be disrupted. Importantly, none of these mechanisms is thought to operate equally from low-mass groups to rich clusters. The high fraction of S0s present in all these dense environments therefore suggests that a combination of these mechanisms may be involved, with varying degrees of importance.

Galaxies in which star formation has been recently suppressed, ∼0.5–1.5 Gyr ago, should be well described by the composite of an A-type stellar population (whose main-sequence lifetime ranges from 0.5 to 1.5 Gyr) and an old population, which was present in the galaxy before the last episode of star formation. This type of galaxies was found for the first time by Dressler & Gunn (1983), and they are conspicuous by the presence of strong Balmer absorption lines in their spectra, characteristic of the A stars, superimposed on to a spectrum of an older (several Gyr) stellar population, and with no emission lines (indicating no ongoing star formation). These galaxies are called either 'k+a', after their dominant stellar types (old 'k' and young 'a'), or 'E+A', indicating their spectra correspond to that of a typical early-type ('E') galaxy with additional A-stars. We will refer to them as 'k+a' galaxies hereafter.

Due to the importance of 'k+a' galaxies as observable instances of rapid evolution, they have been the subject of many studies (Dressler & Gunn 1983; Zabludoff et al. 1996; Norton et al. 2001; et al. 2009, 2012, 2013; Poggianti et al. 2009). Although first discovered in the cluster environment (Sparke, Kormendy & Spinrad 1980; Dressler & Gunn 1983), they have also been found in the field (Zabludoff et al. 1996; Blake et al. 2004) and in groups (Poggianti et al. 2009). Few 'k+a' galaxies are found in the local Universe, but their prevalence increases significantly with redshift, such that in intermediate-redshift clusters they can represent up to 10 per cent of the total galaxy population (Poggianti et al. 2009). In those intermediate-redshift clusters, 'k+a' galaxies tend to avoid the central regions, implying that the suppression of star formation does not require the extreme conditions of cluster cores, and may begin in less dense environments such as groups (Dressler et al. 1999). While 'k+a' galaxies in general often show early-type morphologies (sometimes disturbed; Yang et al. 2008), in clusters they are generally associated with disc-like systems (Caldwell, Rose & Dendy 1999; Tran et al. 2003), and in many cases they also show spiral signatures, implying that the time-scale for the spectral evolution is shorter than that for any morphological transformation (Poggianti et al. 1999).

Analysing the internal spatial distributions, and ideally kinematics, of the different stellar populations inhabiting these galaxies is crucial to understand the mechanisms responsible for the suppression of star formation. If the last episode of star formation took place in the central regions, it would be consistent with processes such as galaxy–galaxy interactions and minor mergers (Mihos & Hernquist 1996; Bekki et al. 2005, but see e.g. Teyssier, Chapon & Bournaud 2010, and the discussion in Section 4 in this paper). In contrast, a more extended young population could imply depletion of a galaxy's gas reservoir through interaction with the hot ICM (Rose et al. 2001; Bekki et al. 2005; Bekki 2009).

To perform such an analysis, we have used integral field spectroscopy, obtained using the Fibre Large Array Multi-Element Spectrograph (FLAMES)-GIRAFFE multi-object spectrograph at the VLT (Pasquini et al. 2002), to analyse 13 galaxies with disc morphologies and strong Hδ absorption in the cluster AC114 (also known as Abell S1077; Abell, Corwin & Olowin 1989) at $z \sim$ 0.3. AC114 has been shown to contain a significant population of blue star-forming galaxies by Couch & Sharples (1987, hereafter CS87), but also to have a substantial general suppression of the star formation (as inferred from Hα emission; Couch et al. 2001), which makes it an ideal laboratory for studying how cluster galaxies are transformed. A previous study of 'k+a' galaxies in this cluster has been carried out by Pracy et al. (2005, hereafter P05). They obtained observations using FLAMES with a very similar configuration, although they did not focus specifically on galaxies with disc morphology. We were not aware that their observations existed when ours were scheduled, but such repeated observations enable us to check the reproducibility of our measurements. Combining the P05 data set with our own also adds some additional galaxies to the sample we consider in this paper. In their study, P05 only consider the spatial distribution of the Hδ equivalent width. We expand on this, measuring the stellar populations in more detail and considering the resolved galaxy kinematics.

Throughout this paper we assume a cosmology with $\Omega_{\rm m} = 0.3$, $\Omega_\Lambda = 0.7$, $H_0 = 70 \, {\rm km \, s^{-1} \, Mpc^{-1}}$.

2 DATA

2.1 Sample

The current sample consists of 13 galaxies, observed and identified by CS87 as members of the cluster AC114 at $z \sim 0.31$. The CS87 catalogue provides redshifts and spectral line measurements, as measured on 8 h integrations with the 3.9 m Anglo-Australian Telescope, using a spectrograph with a spectral resolution $R \sim 1400$ and fed by 2.6 arcsec diameter fibres. AC114 also has wide-field archive *Hubble Space Telescope* (*HST*) WFPC2 imaging, which is used to catalogue the morphological make-up of AC114 in Couch et al. (1998, hereafter C98). Based on the combined CS87/C98 catalogue, the sample galaxies were selected to have Hδ rest-frame equivalent width EW(Hδ) > 3 Å (the sign convention here is that a positive EW for Hδ means absorption), which is the common criterion to be considered 'k+a' (Poggianti et al. 1999), disc morphology and magnitude $R_{\rm F} \leq 20.5$. Some further sample limitations were imposed by the spectrograph's field-of-view and restrictions on the placement of each integral field unit (IFU) in order to avoid button collisions and crossed fibres.

Nine of the objects selected to be observed show no [O II]λ3727 emission in the CS87 catalogue, and hence correspond to a true 'k+a' selection. The remaining four show some [O II]λ3727

Table 1. Identity number of the galaxy from Couch & Newell ([1984](#)), coordinates, morphologies, Galactic reddening-corrected colours and distance to the cluster centre for the galaxies in our sample (top) and the P05 sample (bottom). At $z = 0.3$ one arcsec corresponds to 4.454 kpc. Galaxies labelled with * have detected emission in [O II]λ3727. Galaxies labelled with 'P05' are present in both samples.

Target	α_{J2000} (h m s)	δ_{J2000} (° ′ ″)	Morphology	$B_{\rm J} - R_{\rm F}$	$R_{\rm cl}$ (Mpc)
CN24	22 58 50.0	−34 47 57	Disc	2.4	0.10
CN74*	22 58 44.6	−34 49 11	Disc	1.26	0.34
CN119	22 58 42.3	−34 47 41	Disc	2.44	0.48
CN143^{P05}	22 58 42.8	−34 48 31	Disc	1.67	0.32
CN146*	22 58 49.7	−34 52 13	Disc	1.42	0.34
CN155*	22 58 43.4	−34 49 37	Disc	1.43	0.48
CN187^{P05}	22 58 50.5	−34 49 12	Disc	2.17	0.31
CN191^{P05}	22 58 52.9	−34 48 46	Disc	1.49	0.30
CN228^{P05}	22 58 46.5	−34 46 18	Disc	1.39	0.50
CN232	22 58 59.5	−34 51 46	Disc	2.34	0.50
CN243*	22 58 40.7	−34 46 44	Disc	1.58	0.56
CN254	22 58 39.8	−34 47 50	Disc	1.99	0.48
CN849^{P05}	22 58 37.3s	−34 48 20	Disc	1.8	0.61
CN4	22 58 40.7s	−34 47 53	Elliptical	2.48	0.42
CN22	22 58 50.0s	−34 48 13	Peculiar	1.48	0.09
CN89	22 58 48.9s	−34 46 57	Elliptical	2.24	0.32
CN229	22 58 45.3s	−34 46 21	Disc	2.3	0.51
CN247	22 58 39.6s	−34 47 15	Elliptical	2.46	0.53
CN667	22 58 41.0s	−34 46 21	Disc	1.6	0.62
CN858	22 58 48.0s	−34 47 26	Elliptical	2.35	0.19

emission, indicating that they have ongoing star formation, though possibly declining given their Hδ EW, or host an active galactic nucleus (AGN).

In addition to these galaxies, we include in our analysis the objects observed by P05. This sample was selected from the same cluster in a similar manner to that described above, except that no restriction was placed on morphology and none of their galaxies had detected [O II]λ3727 emission. Six galaxies from our selection were also observed by P05, as well as two additional disc galaxies, four ellipticals and one peculiar galaxy. The combined sample therefore comprises 20 galaxies, of which 15 possess disc morphology.

Note that, for galaxy CN849, the flux present in our observations was very low. This was found to be due to an incorrect target position. Fortunately, this galaxy was also included in the P05 data sample and could be analysed using that data. Also, when comparing the redshifts measured for the galaxies observed by both P05 and ourselves we discovered an inconsistency for CN254. Inspecting the coordinates we discovered that the galaxy labelled CN254 in P05 is actually CN229, another disc galaxy at $z = 0.319$. The cross-comparison sub-sample with multiple observations therefore comprises four objects.

In Table [1](#), we list all of the objects considered in this paper, with their coordinates, morphologies, colour ($B_{\rm J}$–$R_{\rm F}$, corrected for Galactic reddening) and projected distance to the cluster centre.

2.2 Observations

The observations were obtained at the VLT-UT2 using the FLAMES in GIRAFFE mode at a resolution of $R \sim 9600$. With this setup, 15 individual IFUs were deployed over the whole field of view, with two of them being dedicated to the sky to ensure a reliable sky subtraction. Each IFU consists of 20 squared microlenses of

0.52 arcsec on a side, making up a surface of 3×2 arcsec^2 per IFU, which corresponds to $\sim 14.0 \times 9.3$ kpc^2 at the distance of AC114 ($\sim 2.3 \times 2.3$ kpc^2 per spaxel).

The total exposure time was ~ 13 h, distributed in 14 exposures in different nights of 2004 June, August and December . Observations were taken with seeing conditions within the requested service mode constrain (≤ 0.8 arcsec) and seeing ranged from 0.49 to 1.06 arcsec. The observed wavelength range was 5015–5831 Å, which at a redshift of $z \sim 0.3$ corresponds to 3850–4394 Å in rest frame, covering the K and H calcium features (3934 and 3969 Å), the Balmer lines Hδ (4102 Å) and Hγ (4341 Å) and the G band (4305 Å). At that wavelength range, the instrumental resolution is 0.57 Å sampled with 0.2 Å pixels, yielding a velocity resolution of $\sigma = 10$ km s^{-1} at $z \sim 0.3$. Since we expect $\sigma \geq 50$ km s^{-1}, this resolution is enough to comfortably resolve the lines.

In order to ensure an accurate calibration of the data set, we obtained arc lamp and Nasmyth flat-field images immediately after each science exposure.

The observations by P05 were obtained with an identical setup, though with slightly lower integration times. The seeing values for these observations ranged from 0.54 to 0.84 arcsec. Their independent spectra for the four galaxies we have in common provide a useful check of the robustness of our results.

2.3 Data reduction

The data were reduced using the GIRAFFE pipeline provided by European Southern Observatory (ESO) (Izzo et al. [2004](#)). The pipeline first subtracts the bias and the overscan regions. Then, using the corresponding Nasmyth flat-field image, it determines the position and width of the spectra on the CCD and simultaneously produces a normalized flat-field to account for the variations in transmission from fibre to fibre. Because the observations were taken with the original CCD, which was only changed in 2008 May, removal of the dark was necessary due to the presence of a prominent glow in the CCD. A dispersion solution was created using the corresponding ThAr arc lamp frame, and the spectra rebinned to a constant dispersion. No flux calibration was required for the analysis of the data.

The pipeline did not include a recipe for the subtraction of the sky. Therefore, the subtraction was done combining all fibres from the two IFUs dedicated to the sky, together with the single sky fibre associated with each IFU, giving a total of 52 fibres. We noticed that one of the sky IFUs was systematically too bright, perhaps due to contamination by a low surface brightness object, resulting in an oversubtraction of the sky in our object fibres. We decided to exclude this IFU and use the remaining 32 sky fibres for the sky subtraction.

For consistency, we obtained the raw data for the P05 observations from the ESO archive and reduced them in the same manner as our own observations.

2.4 Stellar population and kinematic analysis

To extract information about the kinematics and stellar populations of the galaxies, we used the penalized pixel fitting PPXF software described in Cappellari & Emsellem ([2004](#)). This algorithm uses a maximum-likelihood approach to fit the spectra in pixel space, simultaneously determining both the stellar kinematics and the optimal linear combination of spectral templates required to match the input spectrum. We employed two separate collections of templates, one drawn from the ELODIE 3.1 stellar library (Prugniel

et al. 2007) and the other containing PEGASE-HR simple stellar population (SSP) models (Le Borgne et al. 2004). The latter spectra are constructed using the ELODIE library, and hence both have the high resolution and wavelength coverage required to fit our spectra [0.5 Å full width at half maximum (FWHM) and 4000–6000 Å, respectively]. Internally, PPXF convolved the template spectra with a Gaussian in order to match the spectral resolution of our observations. We restricted the templates to two classes (II–III and V) for each stellar type OBAFGKM, and to SSPs with 12 different ages logarithmically distributed between 1Myr and 15 Gyr and five different metallicities [Fe/H] ranging from -1.7 to 0.4.

For each spectrum, the program outputs the velocity, V, and velocity dispersion, σ, together with a refined estimate of the redshift. The values obtained for the kinematics when using the stellar library templates and those obtained using the SSP models were, in general, very similar. However, for some of the galaxy spectra, occasional noise features present in the stellar library templates spectra resulted in obviously discrepant fits and wrong values for the kinematics. In these cases, we only use the results obtained using the SSP models. Errors in the kinematic parameters obtained with PPXF were estimated in the recommended manner, by performing Monte Carlo simulations on the original spectra with added noise.

In addition to the kinematics, PPXF also provides the weights of the templates which provide the best fit to the observed spectrum. These weights, after normalization, represent the fractional contribution of each template to the total luminosity. Below we use the weights obtained using the stellar library and the SSP models

separately, in order to study the distribution of different stellar types and stellar populations throughout our sample galaxies.

3 ANALYSIS

We begin by studying the global properties of the sample, by integrating the fibres from each IFU to produce a single spectrum per galaxy. For most of the sample we combined all the fibres. However, in a few cases this resulted in an excessively noisy spectrum, and therefore only fibres with signal-to-noise ratio (S/N) $\gtrsim 5\,\text{Å}^{-1}$ (defined in selected regions of the continuum) were then combined. The rejected fibres were always far from the brightest pixel, in the outskirts of the target galaxy.

In Fig. 1 we plot the integrated spectra for a representative subsample of the galaxies: CN191, CN232, CN143 and CN74. The S/N of the integrated spectra were relatively high, reaching values of $\sim 22\,\text{Å}^{-1}$ (CN146). All of the spectra display the K and H calcium lines and the *G* band, which are characteristic of an old population. However, the Hδ and Hγ absorption lines, produced by the young, A-star population, are only strong in two of the spectra. The lack of strong Balmer absorption in the remainder contrasts with their selection as 'k+a' galaxies. Below we measure the Hδ index of the galaxies in order to quantify the strength of this feature.

We are also interested in considering spatially resolved information from the different regions of the galaxies covered by the IFUs. In the majority of the galaxies at least some of the central fibres had sufficient S/N (reaching values of $\sim 15\,\text{Å}^{-1}$) to be analysed individually, although the degree to which this is possible varies
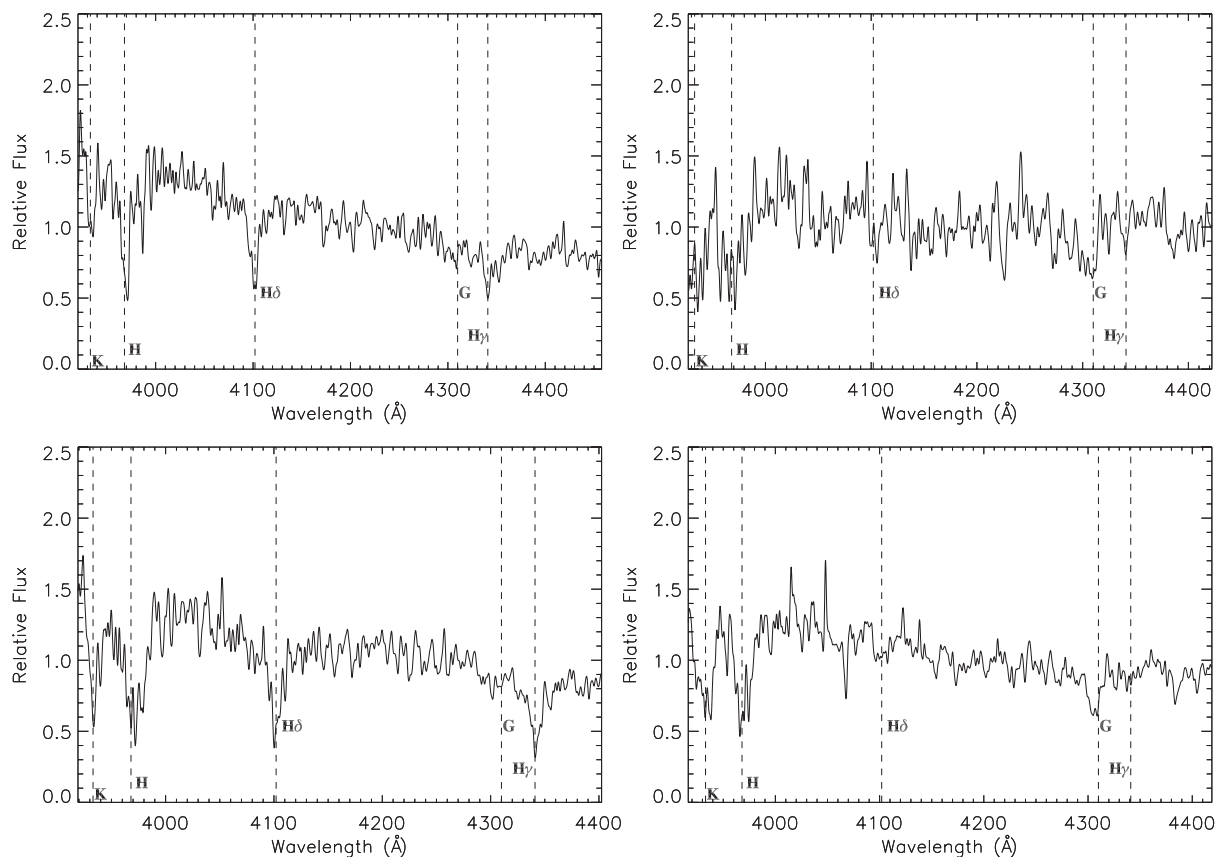
Figure 1. Integrated spectra for a representative sample of our galaxies, from left to right and top to bottom: CN191, CN232, CN143 and CN74. We provide two examples of targets with prominent Balmer absorption (left) and two targets without (right). The spectra have been smoothed with a Gaussian of FWHM 1 Å to improve their presentation. Note that the spectra have not been flux calibrated.

Table 2. Galaxy ID, redshifts, young population indicators, velocity dispersions, V_{rot}/σ and state of interaction for the galaxies in our sample (top) and the P05 sample (bottom). Note that morphology and colour are listed in Table 1. Galaxies labelled with * have [O II]λ3727 detected emission by CS87.

Target	z	$H\delta_F$ (Å)	A/(AFGKM) (± 0.2)	f_{young} (± 0.2)	σ_{int} (km s^{-1})	V_{rot} (km s^{-1})	V_{rot}/σ_{int}	Interacting
CN143	0.310	6.7 ± 0.7	0.7	1.0	107 ± 15	133 ± 18	1.2 ± 0.2	No
CN191	0.305	5.1 ± 0.3	0.4	0.7	61 ± 8	137 ± 51	2.2 ± 0.9	No
CN155*	0.320	5.0 ± 0.3	0.4	0.9	282 ± 72	–	–	Yes
CN228	0.317	4.6 ± 0.4	0.8	0.2	210 ± 66	177 ± 38	0.8 ± 0.6	Yes
CN146*	0.300	3.7 ± 0.3	0.7	0.0	184 ± 20	–	–	No
CN243*	0.326	3.1 ± 0.3	0.3	0.5	232 ± 19	–	–	Yes
CN254	0.309	2.1 ± 0.5	0.0	0.0	202 ± 26	166 ± 20	0.8 ± 0.2	No
CN232	0.315	1.1 ± 0.6	0.0	0.0	185 ± 32	137 ± 55	0.7 ± 0.3	No
CN24	0.322	1.0 ± 0.4	0.0	0.0	93 ± 12	–	–	No
CN74*	0.316	1.0 ± 0.3	0.0	0.0	239 ± 88	152 ± 75	0.6 ± 1.6	No
CN187	0.308	1.0 ± 0.5	0.0	0.0	202 ± 24	–	–	No
CN119	0.308	0.9 ± 0.5	0.2	0.4	144 ± 134	–	–	No
CN22	0.336	6.4 ± 0.4	0.6	0.7	83 ± 22	83 ± 21	1.0 ± 1.0	Yes
CN849	0.324	2.3 ± 0.4	0.1	0.2	189 ± 7	86 ± 11	0.5 ± 0.3	Yes
CN89	0.317	2.1 ± 0.9	0.0	0.0	94 ± 40	–	–	No
CN247	0.319	1.0 ± 0.4	0.0	0.0	214 ± 10	–	–	Yes
CN667	0.312	0.6 ± 0.4	0.0	0.0	128 ± 18	–	–	Yes
CN229	0.320	0.3 ± 1.1	0.2	0.1	186 ± 97	–	–	No
CN4	0.308	-0.3 ± 0.3	0.2	0.2	185 ± 20	–	–	No
CN858	0.312	-1.2 ± 1.7	0.0	0.0	182 ± 52	–	–	No

between galaxies. For this reason, in addition to performing the analysis for the individual fibres, in each galaxy we combined all the pixels immediately adjacent to the brightest one, which we refer to as the 'surroundings' (covering from ~1.6 to 3.2 kpc), and those placed further away, which we define as the 'outskirts' (~3.2 to 4.8 kpc). In some cases, due to the low S/N in the pixels far away from the centre, we could not obtain reasonable quality spectra for the 'outskirts'.

To find the centre of each galaxy we built images of the light distribution in the continuum region between the Hδ feature and the sky line at λ5577 for each IFU. The centre of the galaxy was associated with the brightest (and hence usually highest S/N) pixel. Some large and inclined galaxies were purposefully offset to include their outer regions in the IFU. However, many of the other galaxies also display offsets from the IFU centre. These offsets, which are also present in the observations carried out by P05, are likely a result of inaccuracies in the astrometry and IFU positioning errors. They are, however, significantly smaller than the field of view so do not compromise the analysis.

3.1 Indicators of a young population in the 'k+a' galaxies

3.1.1 Line index measurements

As explained above, 'k+a' spectral features arise from the truncation of star formation in a galaxy, which may be preceded by a starburst, and reflect the composite of a young and an old stellar population. These galaxies are usually identified by the strong Balmer absorption lines in their spectra. Since the higher-order Balmer lines are less affected by emission from ionized gas (Osterbrock 1989), the most commonly used indicator is the Hδ line at 4102 Å, which is also conveniently located in the optical part of the spectrum at low and intermediate redshift. Although the selection criteria do vary depending on the study, 'k+a' galaxies are generally selected to have EW(Hδ) > 3 Å and no detected emission lines.

The strength of the Hδ absorption line is related to the mechanism responsible for the 'k+a' feature. Poggianti et al. (1999) showed that strong Hδ absorption lines [EW(Hδ) > 4–5 Å] can only be caused by the abrupt truncation of star formation after a starburst. Lower values of [EW(Hδ)] can also be achieved by a simple truncation of a continuous and regular star formation in the galaxy. However, the strength of the Hδ line subsides with time, so it is difficult to distinguish between recent truncation and an older one that was preceded by a starburst.

Although we consider more sophisticated indicators of the stellar population later in this paper, given the importance and simplicity of the Hδ absorption feature, we first measure the equivalent width of this line for the sample galaxies. We utilized the redshifts obtained from the template fits with PPXF (Section 2.4), as listed in Table 2. Equivalent widths were measured using the software INDEXF (Cardiel 2010), which uses the Lick/IDS index definitions of Worthey & Ottaviani (1997) to measure the signal within the line with respect to the neighbouring continuum. To make our results comparable with those obtained by P05, we use the index Hδ_F, which takes the continuum intervals 4057.25–4088.5 Å and 4114.75–4137.25 Å around the central 4091.00–4112.25 Å bandpass. Errors are estimated from the propagation of uncertainties in the spectra and the measured radial velocities.

Four of the galaxies in our sample display emission lines, which would affect the line index measurement due to the filling of the absorption lines. To avoid this, for these four galaxies instead of using the original spectrum we measured the line index on the best-fitting spectrum constructed by PPXF. This procedure has been shown to produce very good results by Johnston et al. (2013b).

The values of Hδ_F for all the galaxies in our sample are listed in Table 2. We also list the values obtained for the galaxies from the P05 sample. For galaxies that are present in both samples we obtained very similar values, consistent within the given uncertainties. Hereafter we used the values measured in our data, because they possess higher S/N ratios.

The first surprising finding is the number of galaxies for which we measure $H\delta_F$ lower than 3 Å. This was already suggested from the weak Balmer absorption lines apparent in some of the spectra upon visual inspection (see Fig. 1). These low values contrast with those expected from the spectroscopic study by CS87, in which all of our sample showed EW($H\delta$) higher than 3 Å. This discrepancy was also found by P05. It appears that the uncertainties in the CS87 $H\delta$ EWs are rather large, and hence their spectral classifications are only reliable for the most extreme 'k+a' cases.

From our analysis, only seven of the 20 galaxies display EW($H\delta$) > 3 Å, with three of them also having detected [O II]λ3727 emission. If we consider also those with EW($H\delta$) > 2 Å, three more galaxies are included, giving a total of 10. The values obtained in our analysis of the P05 sample are in reasonable good agreement with what they found, considering that each study applied a different method. We only found one galaxy, CN849, where we measured a lower value of $H\delta_F$ (2.3 ± 0.4) than what they obtained (3.6 ± 0.3), which in this case is significant because it changes the galaxy's 'k+a' classification.

As mentioned above, four of the galaxies we observed are listed as having [O II]λ3727 emission in CS87 and therefore do not meet the standard 'k+a' criteria. Their EW([O II]) values range from 7.6 Å to 39.6 Å. These are likely reliable emission line identifications. Three of them are found to have $H\delta_F$ > 3 Å (CN146, CN155 and CN243) and they also show signs of emission in $H\gamma$ and $H\delta$ in our data. However, it is not clear whether these emission lines result from residual star formation or AGN activity.

One would expect that if star formation has been recently truncated in those galaxies with strong $H\delta$ absorption, they should have bluer colours due to the presence of the young population. To test this, in Fig. 2 we plot $H\delta_F$ versus $B_J - R_F$ for all the sample galaxies. Objects with strong $H\delta$ absorption are conspicuously bluer than those with weaker $H\delta$ absorption. CS87 also present this plot, finding a consistent trend, though somewhat weaker, presumably due to the larger uncertainties on their EW($H\delta$) estimates. This trend gives compelling support that the galaxies in our sample with stronger $H\delta$ absorption, and particularly EW($H\delta$) $\gtrsim$ 2, contain younger stellar populations.

In Fig. 2 we also indicate the galaxies which have observed [O II] emission. Recall that, for these galaxies, EW($H\delta$) was measured on the template fits produced by PPXF, rather than the data itself,
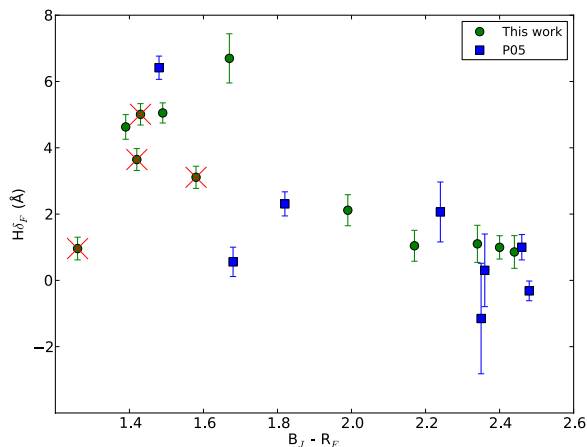
to avoid the effect of line-filling. It is possible that in the case of the bluest galaxy the line-filling has affected the PPXF fit itself, resulting in an underestimate of EW($H\delta$). These four galaxies are not strictly 'k+a' systems; they may simply be normal star-forming galaxies, although their high EW($H\delta$) might indicate some recent suppression of their star formation. Nevertheless, we retain them in the analysis because they probably lie just outside the boundaries of the 'k+a' class, and may provide useful clues on the process by which galaxies become 'k+a' systems.

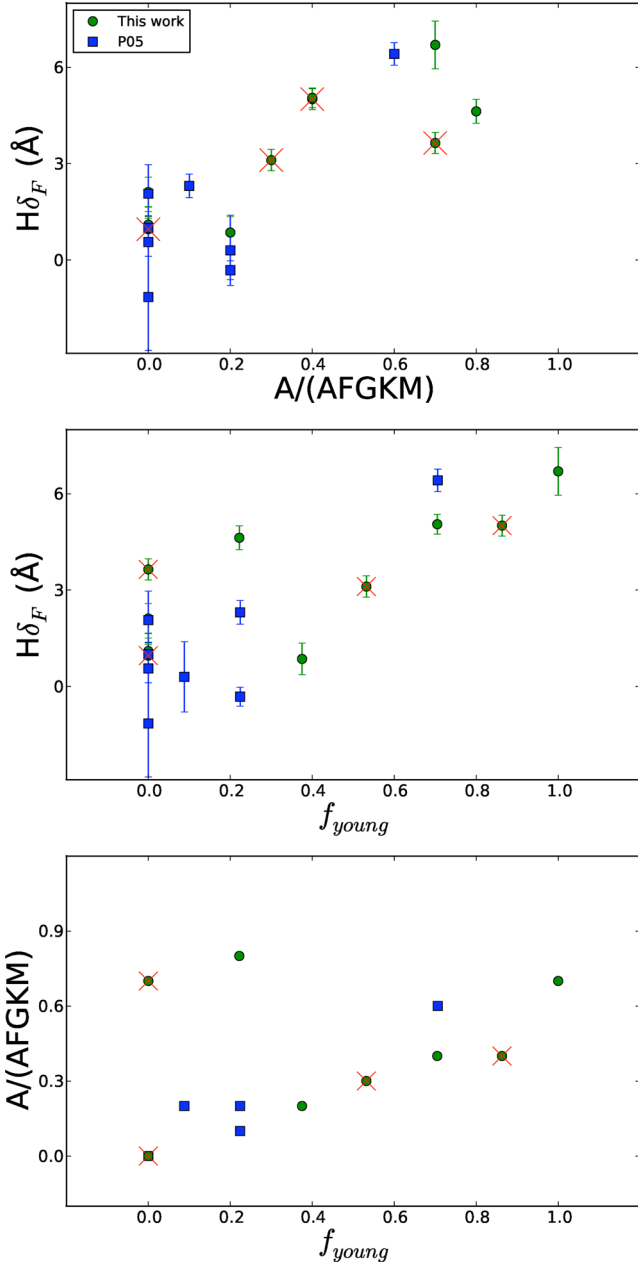### 3.1.2 A/(AFGKM) and f_{young} measurement

Although strong $H\delta$ absorption is the standard indicator of a young population in 'k+a' galaxies, this simply reflects the presence of a substantial stellar population with ages between 0.5 and 1.5 Gyr, whose light is dominated by A stars, but an absence of younger populations containing OB stars, powering nebular emission from H II regions. The presence of this intermediate-age stellar population may also be inferred using other, more quantitative, methods. One approach is template fitting, which uses the full wavelength range available and accounts for the fact that populations of all ages contribute to EW($H\delta$) (and other spectral features). We use the results of template fits performed using PPXF, as described in Section 2.4.

To estimate the relative proportion of each stellar population, we use the normalized light-weighted proportions assigned to the various templates in the best-fitting model.

From the weights obtained using the stellar library templates we determine the fractions of each stellar type (OBAFGKM) contributing to the galaxy spectrum. For the fits using the SSP models, we group the templates into four age bins: 'Age < 0.5 Gyr', '0.5 < Age < 1.5 Gyr', '1.5 < Age < 7 Gyr' and 'Age > 7 Gyr'. One expects an approximate correspondence between the stellar types and SSP ages: stars formed very recently (OB) will dominate the Age < 0.5 Gyr bin, stars with lifetimes ~1 Gyr (main sequence A and F stars) will dominate the '0.5 < Age < 1.5 Gyr' bin, and longer-lived stars (GKM) will correspond to the two older age bins. However, the stellar population templates contain contributions from stars of all types with lifetimes longer than the SSP age.

To evaluate the fraction of A-type stars we use the ratio A/(AFGKM). OB stars are excluded from this fraction because their presence is ill-constrained by our fits, due to their featureless spectra together with the uncertain flux calibration and limited wavelength range of our data. Also, OB stars do not contribute significantly to the stellar mass of a galaxy. For the stellar populations, our primary quantity is the fractional contribution of SSPs with 0.5 < Age < 1.5 Gyr over the total, hereafter f_{young}. The values of A/(AFGKM) and f_{young}, determined with the integrated spectra for each galaxy, are listed in Table 2.

Thus now we have three different indicators of the presence of a young populations in these galaxies, $H\delta_F$, A/(AFGKM) and f_{young}. Comparing these parameters provides a useful indication of their robustness, and therefore the reliability of using only one of them in cases when the other ones cannot be obtained. This comparison is done in Fig. 3, where we plot A/(AFGKM) and f_{young} against $H\delta_F$ for our entire galaxy sample. Uncertainties on the $H\delta_F$ measurements are indicated, but PPXF does not provide error estimates for the template weights. We therefore estimate average uncertainties for A/(AFGKM) and f_{young} from the standard deviation of the scatter from a linear correlation with respect to $H\delta_F$ after subtracting the contribution to their error by $\Delta H\delta_F$. We obtain an uncertainty in both quantities of 0.2. which is also noted in Table 2.

Figure 2. $H\delta_F$ versus $B_J - R_F$ colour for our entire galaxy sample. In the case of objects that were observed by both P05 and ourselves, we only plot our values. Galaxies with detected emission in [O II] by CS87 are indicated by a red cross.

Figure 3. Values of A/(AFGKM), f_{young} and Hδ_F plotted against each other for our sample (green circles) and measured by us on spectra obtained by P05 (blue squares). For galaxies that are present in both samples we only plot values measured in our data because they have higher S/N. We only plot error bars in Hδ_F, as PPXF does not provide uncertainties on the weights in the best-fitting combination of templates. Galaxies with detected emission in [O II] by CS87 are indicated by a red cross. In the plot of f_{young} versus A/(AFGKM) there are fewer visible points because they are superimposed on to each other.

As expected, there is a good correlation between these quantities. Galaxies with strong Balmer absorption lines also show high fractions of A/(AFGKM) and f_{young}, while those with weak Hδ_F show very low values of A/(AFGKM) and f_{young}. The fractions of A/(AFGKM) and f_{young} also present good correlation between them. More quantitatively, for A/(AFGKM) and Hδ_F we obtain a Spearman's correlation coefficient $\rho = 0.65$, while for f_{young} and Hδ_F, $\rho = 0.56$. In the case of A/(AFGKM) and f_{young}, $\rho = 0.76$. The chance of any of these correlations being spurious is $\lesssim 1$ per cent.

3.2 Spatial distributions

As mentioned previously, in addition to providing global information about a galaxy, integral field spectroscopy allows us to study properties at smaller spatial scales and hence consider different regions within a galaxy. We exploit this possibility by performing the same analysis described above, but now applied both to the spectra from individual IFU elements and to combined spectra from the 'centre', 'surroundings' and 'outskirts' regions of each galaxy.

We have used these results to construct maps of the three different age indicators, Hδ_F, A/(AFGKM) and f_{young}, for each galaxy. In many galaxies, due to the S/N being too low in the 'outskirts', only the 'centre' and 'surroundings' could be analysed. Cases where the three integrated regions could be analysed can be found in the Appendix (CN74 and CN849). An example of this analysis is shown in Fig. 4 for the galaxy CN228, where the three indicators show a high concentration of the young population in the centre of the galaxy. This is particularly clear when considering the 'centre' versus 'surroundings' regions. The values of the individual fibres for A/(AFGKM) and f_{young} also show a high concentration towards the centre, while the individual Hδ_F are less conclusive.

To examine the stellar population in more detail, in Fig. 5 we show the normalized distributions of the different spectral types and SSP ages obtained for different regions of the same galaxy. The two approaches are broadly consistent: a prominent fraction of A-stars is associated with a significant young-age population.
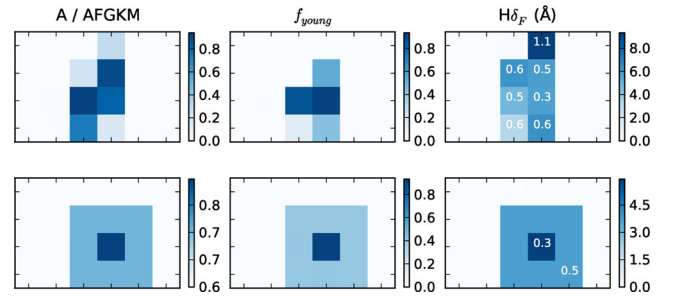

Figure 4. Maps of the individual fibre values of A/(AFGKM), f_{young} and Hδ_F index (top) and the corresponding values for the integrated regions 'centre' and 'surroundings' (bottom) in CN228. Errors of the Hδ_F index are printed over the regions. Each spatial pixel (or spaxel) has a size of 0.52 × 0.52 arcsec^2 which corresponds to ~2.3 × 2.3 kpc^2 at the redshift of AC114.
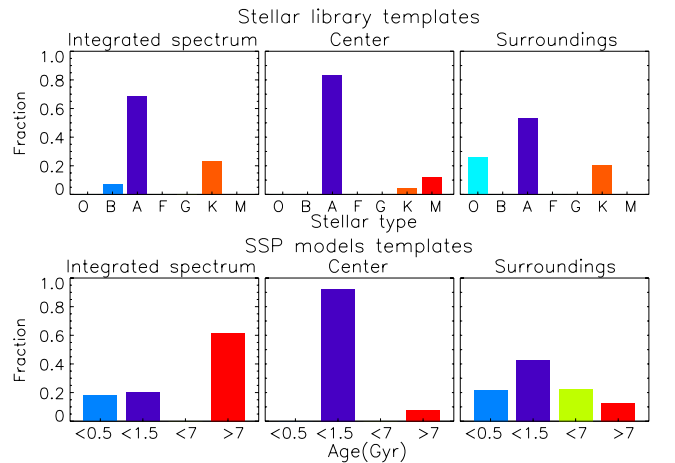
Figure 5. Histograms of stellar type and stellar population age obtained with pPXF for the integrated spectra, 'centre' and 'surroundings' of CN228.
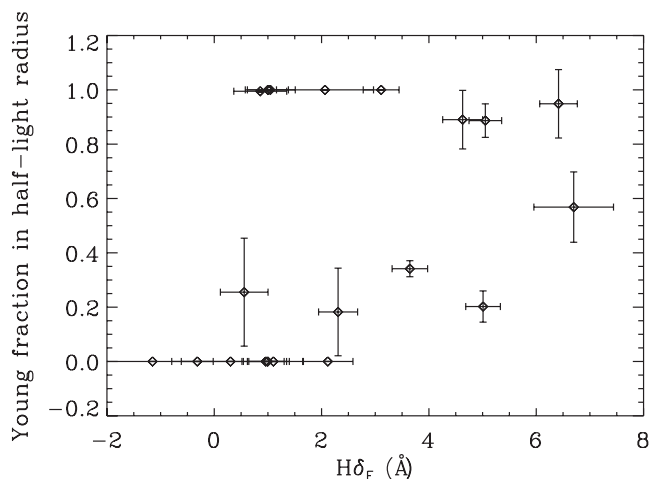
Figure 6. The luminosity-weighted fraction of the young stellar population contained within the half-light radius of the old population plotted against the global Hδ_F. A value of this fraction larger than 0.5 indicates that the young population is more concentrated than the old one (see text for details).

The maps of Hδ_F, A/(AFGKM) and f_{young} for each galaxy are our primary source of information regarding the spatial distributions of the young and old stellar populations. However, the maps are difficult to deal with quantitatively, and there is some subjectivity in identifying the trends they reveal. We have examined these maps in detail, and in the Appendix we present qualitative descriptions of each galaxy, in addition to the maps themselves.

In an attempt to quantify the differences in the spatial distributions of the young and old stellar populations we have used these maps to estimate the luminosity-weighted fraction of the young stellar population contained within the half-light radius of the old population. We have assumed exponential intensity profiles for both populations. A value of this fraction larger than 0.5 indicates that the young population is more concentrated than the old one. Fig. 6 shows this fraction plotted against the global Hδ_F values. There is a large scatter, indicating significant differences in the current properties and formation histories of the galaxies. Nevertheless, galaxies with the strongest Hδ_F seem to show some tendency to have more centrally concentrated young populations. This suggests that the last episode of star formation often took place in the central regions of these galaxies. The sample size, spatial resolution and uncertainties of this study prevent us from reaching a very robust conclusion in this respect, but it is reassuring that our findings are consistent with independent evidence from recent studies of local S0 galaxies (Bedregal et al. 2011; Johnston et al. 2012, 2013a).

3.3 Kinematics

If spiral galaxies are being transformed into S0s by any of the processes discussed in the Introduction, in addition to the changes in stellar populations considered above, their kinematics may also be affected. The kinematics of the 'k+a' galaxies in our sample can therefore indicate what mechanisms are responsible for the truncation of their star formation. If the process acts primarily to starve a spiral galaxy of its gas supply, the disc rotation should be preserved in the resulting galaxy. However, if a merger is involved, the remnant would be expected to show more random motions.

The kinematics of the galaxies analysed here were extracted using the software PPXF, as explained in Section 2.4. First of all, we obtained a value of the overall velocity dispersion σ_{int} for the
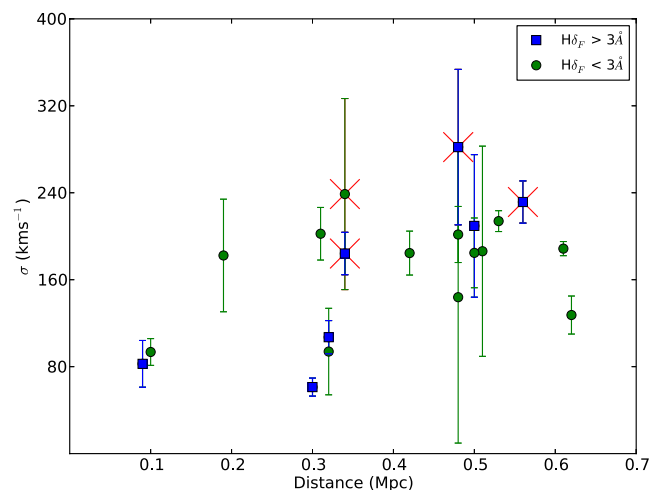

Figure 7. Velocity dispersion σ versus projected distance to the centre of the cluster for galaxies with H$\delta_F > 3$ Å (blue squares) and H$\delta_F < 3$ Å (green circles). For those galaxies that are observed by both P05 and ourselves we plot the mean value. Galaxies with detected emission in [O II] by CS87 have a red cross overplotted.

integrated spectrum of each galaxy, which are listed in Table 2. It should be borne in mind that for the galaxies with detected emission by CS87, the measurement of σ_{int} might be affected by the filling of the absorption lines due to emission. A wide range of values of σ_{int} are found, from ~60 to ~280 km s^{-1}. These overall σ_{int} include contributions from both rotational and random motions, which we will attempt to separate below.

If the gas and the kinematics of the galaxies are being affected by the cluster environment, one would expect galaxies closer to the cluster centre to show different behaviour to those that are further out, as found by Jaffé et al. (2011). To test this, we consider σ_{int} as a function of the projected distance from the cluster centre (Table 1), which is plotted in Fig. 7. For the full sample there does not appear to be any clear trend. However, if we separate galaxies with high (≥ 3 Å) and low (< 3 Å) Hδ_F, we see that those with high Hδ_F (blue squares) present a strong trend. High Hδ_F galaxies have higher σ_{int} the further they are from the cluster centre, while those with low Hδ_F (green circles) show little change with position. Some of the high-Hδ_F and high-σ_{int} galaxies display emission lines (red crosses), which may make the estimation of σ_{int} unreliable. However, if we remove them from the plot, we see that the trend remains.

We now turn our attention to the kinematics of the galaxies on smaller scales, which can be studied using the outputs of fits performed to the individual IFU fibres. We construct line-of-sight velocity, V_{obs}, and velocity dispersion, σ, maps of the galaxies, in a similar manner to those for the young population indicators. An example is shown in Fig. 8 for the galaxy CN228.

We have studied these maps for signs of rotation and differences in velocity dispersion between the central and surrounding pixels. One problem we had to face here was that the 'good' fibres were not always distributed around the brightest pixel in the IFU, and it was sometimes difficult to identify patterns of rotation or velocity dispersion. Since the observed velocity is $V_{obs} = V_{rot} \sin i$, where V_{rot} is the rotational velocity and i the inclination of the galaxy, we need to know the galaxy inclination in order to obtain the actual rotational velocity. The inclination was therefore determined by the apparent ellipticity obtained by fitting an ellipse to the *HST*/WFPC2 images using the IRAF task ELLIPSE. In the case presented in Fig. 8,
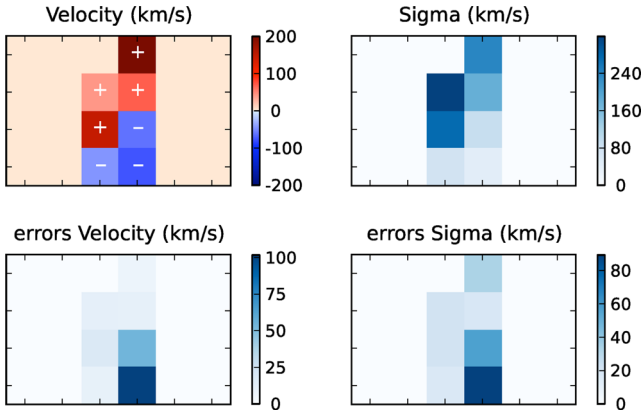
Figure 8. Example of the radial velocity and velocity dispersion maps, with errors plotted below. The plus ('+') and minus ('−') symbols indicate the direction of rotation. In this image we show the example of CN228, showing a clear pattern of rotation and with similar values of σ along the galaxy.
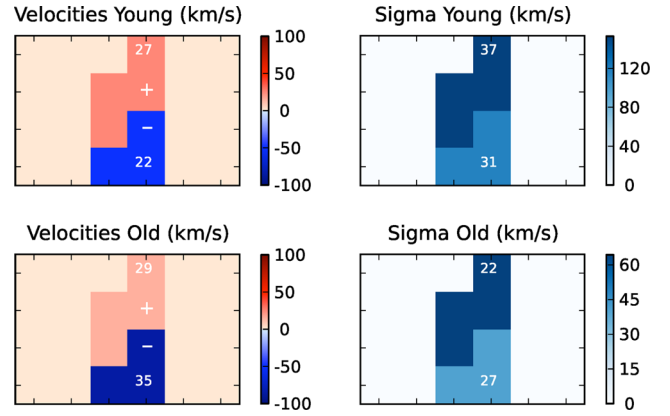

Figure 9. Kinematic decomposition of the young and old stellar populations in CN228, obtained using our two-component fitting method. Mean velocity and velocity dispersion values are presented in the IFU image. The plus ('+') and minus ('−') symbols indicate the direction of rotation. Errors in the fits are plotted over the corresponding regions.

we can see a clear pattern typical of rotation, with $V_{rot} = 177 \pm 38 \, \text{km s}^{-1}$. The distribution of σ is roughly flat.

Previous studies of the kinematics of 'k+a' galaxies have found significant rotation in many of them (Franx 1993; Caldwell et al. 1996; Pracy et al. 2009, 2013; Swinbank et al. 2012), although some are found to be mainly pressure-supported (Norton et al. 2001). We attempted our kinematic analysis in all the galaxies, including the observations of P05, and found that at least eight galaxies display rotation, with values of $V_{rot} \sim 85\text{--}180 \, \text{km s}^{-1}$.

The measured values of σ_{int} and V_{rot} are listed in Table 2, along with their ratio (V_{rot}/σ_{int}), which indicates whether a galaxy is a rotationally (>1) or pressure (<1) supported system. Using this last parameter, we see that two of the systems displaying rotation are clearly rotationally supported, typical of disc-like systems, while five show $V_{rot}/\sigma_{int} < 1$ indicating they are dominated by random motions. Coming back to Fig. 7, now we are able to establish if the high values of σ_{int} found for some galaxies are due to rotation or to random motions. From the 10 galaxies with $H\delta_F \geq 2 \, \text{Å}$, rotation is detected in six of them and dominant in two of these. However, the amount of rotation in galaxies far from the centre, in particular CN254 and CN228, is conspicuously higher ($\geq 160 \, \text{km s}^{-1}$) than in those closer to the centre such as CN143 and CN191 ($<140 \, \text{km s}^{-1}$). The observed trend to lower internal velocities with decreasing distance from the cluster core may therefore indicate a trend to less regular kinematics, and hence environmentally induced disturbances in the centre of the cluster.

3.4 Kinematic decomposition

The kinematics studied in the previous section are derived assuming that all stellar populations contributing to a spectrum have the same kinematics. However, our data afford the possibility of measuring the kinematics of the young and old populations in 'k+a' galaxies separately (e.g. Franx 1993; Norton et al. 2001). Separated kinematics offer a further method of distinguishing between the mechanisms responsible for 'k+a' signature. Rotation in the young components implies it is in a disc and that the galaxy has not been subject to a violent process, particularly if the young population kinematics and distribution are consistent with the older population. On the other hand, a pressure-supported young population implies that a significant interaction has occurred. The degree of rotational support in the old population may then indicate the strength of this interaction.

In order to study the kinematics of the two different populations, we modified the PPXF algorithm in such a way that it could fit two different stellar templates to one spectrum simultaneously, convolving each one with different radial velocities and velocity dispersions. The same modified algorithm has been used to study a galaxy with two counter-rotating discs by Johnston et al. (2013b), with good results. In our case, we used a set of templates containing A-stars and K-stars with different metallicities so that PPXF could clearly distinguish between the two populations.

Decomposing the kinematics is very challenging, and requires higher S/N than available in most of the individual IFU elements. The decomposition was therefore attempted on co-added spectra corresponding to three regions for each galaxy, the centre and both sides, where the orientation of each galaxy is judged from the kinematic maps from Section 3.3. We found that the algorithm was sometimes sensitive to the initial values of V and σ used. We therefore varied these input values and, in order to be considered robust, the outputs of the fits were required to remain constant for a wide range of initial values.

The results are presented in terms of V and σ maps in a similar manner to the previous section. As an example, the kinematic decomposition of CN228 is shown in Fig. 9. In this case, the galaxy is a composite of two populations with similar patterns of rotation, while the young population displays higher values of σ than the old population, throughout the galaxy. As shown previously in Fig. 4, CN228 shows central concentration of the young population in the distribution of the three indicators $H\delta_F$, A/(AFGKM) and f_{young}, implying a concentration of the young population in the centre of the galaxy. Now, adding the information provided by the kinematic decomposition, the fact that this galaxy and others show similar rotation between the young and old population seems to indicate that these were fairly normal disc galaxies which have not experienced a major merger or dominant central starburst. However, the higher σ suggests that they have experienced an interaction which increased the random motions in the gas from which the last population of stars was formed.

In total, three disc galaxies with $H\delta_F \geq 3 \, \text{Å}$ (CN228, CN146 and CN191) and two with $H\delta_F \geq 2 \, \text{Å}$ (CN254 and CN849) could be kinematically decomposed into two populations. In four of these cases both the young and old populations were found to have similar

patterns of rotation, whereas no clear pattern was found in the remaining one (CN146).

The σ values obtained for the two populations display a variety of behaviours, in terms of both their relative strength and their radial gradients. In the case of CN228 discussed above, the σ of the young stars is higher than that of the old population, which suggests that this discy 'k+a' galaxy may have experienced a recent interaction, which has increased the random motions of their cold gas, from which the latest generation of stars have formed, but had less effect on their previously existing stellar populations. Thus, the process cannot be purely gravitational, since the old population is not perturbed, and it must be affecting only the gas (Jaffé et al. 2011). A more detailed analysis of the kinematic decomposition for each galaxy is presented in the Appendix.

3.5 Influence of interactions

Dynamically interacting galaxies are often observed to be experiencing a starburst (e.g. Keel et al. 1985). Simulations have long suggested that mergers and interactions can cause gas in a galaxy disc to lose angular momentum and fall towards the centre of the galaxy, potentially fuelling a central starburst (Barnes & Hernquist 1991; Mihos & Hernquist 1996; Bekki et al. 2005). However, observations often find that interactions promote star formation throughout the galaxies involved (e.g. Kennicutt et al. 1987; Elmegreen et al. 2006), not just in the nuclear region. This can now be reproduced by models which pay closer attention to the role of shock-induced star formation (e.g. Chien & Barnes 2010; Teyssier et al. 2010).

Assuming that the starburst process occurs faster than the replenishment of the gas disc via infall, or alternatively that such infall is suppressed, then following the starburst the galaxy will cease star formation. The resulting galaxy will therefore display a k+a spectrum for a time.

The importance of mergers and interactions as the origin of the 'k+a' feature is supported by studies which find that 'k+a' galaxies (of all morphologies) are more likely to be found with a companion galaxy, when compared to normal galaxies (Goto 2003, 2005; Yamauchi, Yagi & Goto 2008; Pracy et al. 2012). For example, in their catalogue of k+a and their companion galaxies, Yamauchi et al. (2008) found that k+a galaxies were 54 per cent more likely than normal galaxies to have a significant companion. Similarly, the two 'k+a' galaxies with late-type morphology and with a central concentration of the young population studied by Pracy et al. (2012) have nearby companions and could be experiencing tidal interactions. However, note that all of these results are based on the general 'k+a' population, and thus may differ from the discy, cluster 'k+a' population considered in this paper. We have therefore looked for evidence of interactions in the sample.

In Table 2 we have included a column specifying whether each galaxy displays indications of interacting with other objects. This was evaluated by visual inspection of the *HST*/WFPC2 images of the AC114 cluster. Of the 20 galaxies in our sample, seven have a close companion and show clear signs of a merger or interaction. The remainder appear fairly isolated and undistorted. However, the fact that a galaxy does not appear to be currently interacting does not rule out such a process as the cause of a 'k+a' feature. The spectral 'k+a' signature can last for up to 1.5 Gyr, which is enough time for an interacting galaxy to have moved to a completely different region of the cluster and any distortion feature might have faded.

To test if interactions have any influence in the properties of the galaxies, we looked for any kind of correlation with any of the results obtained so far in this study. Of the 10 galaxies with $H\delta >$

2 Å, five show signs of interaction. Of the seven $H\delta > 2$ Å galaxies with discy morphology and usable spatial information, three have centrally concentrated young populations (CN155, CN228 and 849) and all of these show evidence for interactions. In contrast, the four disc galaxies with their young population extended throughout the galaxy do not show any sign of mergers or interactions.

This finding strongly supports a link between dynamical interactions and a centrally concentrated starburst in discy, cluster k+a galaxies. The remainder, with an apparently less concentrated young stellar population, may simply be the result of weaker or older interactions, or caused by an alternative mechanism. However, the strength of $H\delta_F$ for the interacting and non-interacting galaxies does not differ significantly.

4 DISCUSSION

Our analysis reveals that discy 'k+a' galaxies in intermediate-redshift clusters are a mixed population. However, despite the small sample size, we do see some consistent behaviour in a number of important respects. These results are robust to changes in the way we quantify the presence and kinematics of the young and old stellar populations.

The young stellar populations within our sample galaxies are always either distributed similarly to, or more compactly than, the older population. Importantly, however, they are rarely consistent with being purely confined to the galaxy nucleus. Furthermore, the young stars often display rotational kinematics corresponding to the rest of the galaxy, implying they are located in the disc. However, there are some indications that their velocity dispersions are somewhat greater than in normal spiral galaxies.

Together these results suggest that the young stellar component formed in an extended disc, in a manner similar to previous generations of stars in these galaxies. It is not associated with the aftermath of a nuclear starburst, nor star formation in tidally accreted material. However the gas from which the latest stars formed was typically more centrally concentrated than that from which their predecessors were born.

The scenario presented by our data can be brought together with many other pieces of observational evidence to support a consistent picture describing the evolution of the majority of disc galaxies in intermediate-redshift clusters and groups.

First, we note that any satellite galaxy within a larger halo, particularly one massive enough to have developed a quasi-static hot atmosphere (Rees & Ostriker 1977), is very likely to have its own gas halo rapidly removed by interactions with the host halo's intergalactic medium and tidal field, via the mechanisms discussed in the Introduction. The environmental removal of H I gas reservoirs is observed both locally (e.g. Vogt et al. 2004a) and at intermediate redshift (e.g. Jaffé et al. 2012). Star-forming galaxies entering a dense environment (i.e. becoming satellites: low-mass galaxies in groups and higher mass galaxies in clusters) would therefore be expected to gradually decrease their star-formation rate as they consume their remaining supply of dense gas.

However, a gradual decline in the star formation rates of star-forming galaxies in dense environments is at odds with results from large surveys. The colours and Hα equivalent widths of star-forming galaxies are invariant with environment (e.g. Balogh et al. 2004a,b; Baldry et al. 2006; Bamford et al. 2008), although the relative proportions of blue versus red or star-forming versus passive galaxies vary substantially. This strongly implies that galaxies must rapidly transform from star-forming to passive, such that a

transition population is not seen. The transformation mechanism cannot be particularly violent, as many galaxies become passive whilst maintaining their disc morphology, first as red spirals, and then as lenticulars (e.g. Lane et al. 2007; Bamford et al. 2009; Maltby et al. 2012). We must therefore reconcile the need for a rapid transformation in terms of observed colour and emission-line properties, with the requirement that the mechanism only act relatively gently on galaxy structure.

Star-forming galaxies are observed in environments of all densities, though they become much rarer in dense regions. However, it is not yet clear whether those star-forming galaxies which appear to inhabit dense regions are simply the result of projection effects, or whether some galaxies are able to maintain their star formation, at least for a while, in such extreme environments. The former would imply that the transition from star-forming to passive is driven by a deterministic mechanism, specific to particular environments, whereas the latter could permit something more stochastic in nature, in which the effect of environment is simply to increase the likelihood of such a transition (Peng et al. 2010).

A stochastic mechanism, which is not directly related to a galaxy's broad-scale environment, is supported by the observation that the proportions of red or passive galaxies show trends across a wide range of environmental density, and that galaxies with truncated star formation are often associated with groups (Moran et al. 2007; Poggianti et al. 2009; Wilman et al. 2009; Lackner & Gunn 2013), which also host normal star-forming galaxies.

The reality is probably a combination of the deterministic and stochastic pictures, for example a mechanism whose effectiveness depends sensitively on the detailed small-scale substructure of the environment and a galaxy's orbit through it (e.g. Font et al. 2008; Peng et al. 2012). In any case, the deterministic removal of a galaxy's gas halo soon after it becomes a satellite makes the galaxy more vulnerable, helping to reduce the time-scale of any transformation instigated by a subsequent mechanism.

An initial enhancement of star-formation efficiency early in the star-forming-to-passive transformation process will effectively reduce the observability of the transition. The increased star formation efficiency would balance the effect of the declining fuel supply, maintaining the appearance of normality, until the fuel supply is entirely depleted. The galaxy would then immediately cease star formation and rapidly appear passive.

Briefly enhanced or extended star formation in the central regions of cluster spirals is supported by our results, as well as the prevalence of cluster galaxies with 'k+a' spectral types (Poggianti et al. 2009) and more centrally concentrated young populations in spirals (Caldwell et al. 1996; Koopmann & Kenney 2004a,b; Vogt et al. 2004a,b; Bamford et al. 2007; Crowl & Kenney 2008; Rose et al. 2010; Jaffé et al. 2011; Bösch et al. 2013a) and S0s (Bedregal et al. 2011; Johnston et al. 2012; contrary to earlier results, e.g. Fisher, Franx & Illingworth 1996), as well as hints of a brightened population in the Tully–Fisher relation (Bamford et al. 2005; Bösch et al. 2013b). Simulations demonstrate similar behaviour (e.g. Kronberger et al. 2008). The process responsible for a more centrally concentrated young population could be either fading of the external parts of the galaxies or pushing the gas inwards.

Recent studies have found disturbed kinematics in the emission-line gas in cluster spirals, from which their final generation of stars would be expected to form (Jaffé et al. 2011; Bösch et al. 2013a). The increased central concentration of the young population in many of our galaxies is certainly consistent with a decrease in the degree of rotational support. Unfortunately, the quality of our data makes it hard to directly determine whether the relative velocity

dispersion of the young stars in the cluster spirals is higher than that of the old stellar populations. However, together these results suggest that future studies of cluster S0s may expect to find that the most recent disc stellar population has a smaller scale length (and possibly greater scale height) compared to previous generations, implying the presence of a young, small, thick disc. Such a feature may also be interpreted as a lens or additional exponential bulge.

Dust may also play a role in accelerating the progression of the observational signatures that would be associated with a transition. The central concentration of star formation, as described above, to the dustier inner regions of galaxies (Driver et al. 2007) results in a greater fraction of that star formation being obscured from optical indicators (Wolf et al. 2009). The transition stage may thus be hidden from optical studies, but a population of dusty, red galaxies forming stars at a significant, though possibly suppressed, rate is revealed by observations at longer wavelengths (Gallazzi et al. 2009; Geach et al. 2009).

Our results indicate that galaxy–galaxy interactions may be associated with stronger or more recent truncated starbursts, and hence may be a significant transition mechanism. We therefore support the conclusions of Moran et al. (2007), that a combination of galaxy–galaxy interactions, ram-pressure stripping, and other more minor mechanisms are responsible for spiral to S0 transformation.

Galaxy–galaxy interactions have long been theoretically associated with strong bar formation and nuclear starbursts (e.g. Mihos & Hernquist 1996). However, due to the high relative velocities of galaxies in a dense environment, tidal interactions can also have a relatively gentle effect (Moore et al. 1996). There is growing observational evidence that even pair interactions may not cause nuclear starbursts as readily as anticipated, enhancing star formation in spiral arms instead (e.g. Casteels et al. 2013). Furthermore, bars are found to be prevalent in gas-poor, red spirals (e.g. Masters et al. 2011, 2012), and so may be more associated with the suppression of star formation, rather than its enhancement.

The final argument for a spiral to lenticular transformation is the properties of the final galaxies. Lenticulars are consistent with being formed from faded spirals in terms of their Tully–Fisher relation (Bedregal, Aragón-Salamanca & Merrifield 2006), globular cluster specific frequencies (Aragón-Salamanca et al. 2006). However, they do tend to be more bulge dominated (Christlein & Zabludoff 2004) and have hotter discs than spiral galaxies (Cortesi et al. 2013). This can be achieved by an enhancement of central star formation prior to transformation, and a marginal increase in pressure support, perhaps through an accumulation of galaxy–galaxy interactions. Both of these processes are suggested by our results and many of the other studies discussed above. The clearing of dust in the central regions during the transition from spiral to S0 may also enhance the bulge-to-disc ratio (Driver et al. 2007). Separately measuring the stellar population properties of bulges and discs for large samples of spiral and S0 galaxies, in both spectroscopic (e.g. Johnston et al. 2012) and multi-band photometric data (e.g. Simard et al. 2011; Lackner & Gunn 2012; Bamford et al. 2012; Häußler et al. 2013), will help to fill in many of the missing details.

5 CONCLUSIONS

The transformation from spiral galaxies into S0s, if it actually occurs, must comprise a spectral transformation, resulting from the suppression of star formation in the disc of the galaxy; a morphological transformation, in terms of the removal of spiral features from the disc and growth of the bulge; and a modest dynamical

transformation, with a small increase in the ratio of pressure versus rotational support.

We have studied the significance of discy 'k+a' galaxies, indicative of a spiral galaxy in which star formation was truncated ~0.5–1.5 Gyr ago, as the possible intermediate step in the transformation of star-forming spirals into passive S0s in the intermediate-redshift cluster environment.

These galaxies are typically identified by their strong Balmer absorption line equivalent widths, an expected signature of a dominant ~1 Gyr old stellar population. We have used spectral template fitting to show that galaxies selected via the $H\delta_F$ index do, indeed, contain significant fractions of A-type stars and stellar populations with ages between 0.5 and 1.5 Gyr. We study the spatial distribution of the young population using these different indicators, finding generally consistent results. While the discy 'k+a' galaxies appear to be a rather mixed population, their final episode of star formation is always distributed over a region of size similar to, or somewhat smaller than, the older stars.

We have coarsely measured the velocity field of these galaxies, both in terms of the full stellar population and, in a limited number of cases, the separate young and old populations. The results support the picture that, in the majority of our sample, the last generation of stars formed in a disc, in a very similar manner to previous generations.

None of the discy 'k+a' galaxies in this intermediate-redshift cluster appears to have experienced a violent event, such as a merger or significant nuclear starburst, prior to the truncation of their star formation. Instead, their regular disc star formation has simply ceased with only, in some cases, a small increase in central concentration beforehand.

A relatively gentle mechanism must thus be responsible for the cessation of star formation. Gas-related mechanisms, such as ram-pressure stripping, are therefore favoured. However, there is also an indication that many of our galaxies with more centrally concentrated young populations have experienced recent galaxy–galaxy interactions. This raises the possibility that, thanks to prior removal of the gas halo, stochastic gravitational interactions may provide the necessary impetus to halt star formation, perhaps via a brief period of central enhancement.

REFERENCES

Abadi M., Moore B., Bower R., 1999, MNRAS, 308, 947
Abell G., Corwin H., Olowin R., 1989, ApJS, 70, 1
Aragón-Salamanca A., Bedregal A. G., Merrifield M. R., 2006, A&A, 458, 101
Baldry I. K., Balogh M. L., Bower R. G., Glazebrook K., Nichol R. C., Bamford S. P., Budavari T., 2006, MNRAS, 373, 469
Balogh M. et al., 2004a, MNRAS, 348, 1355
Balogh M. L., Baldry I. K., Nichol R., Miller C., Bower R., Glazebrook K., 2004b, ApJ, 615, L101
Bamford S. P., Milvang-Jensen B., Aragón-Salamanca A., Simard L., 2005, MNRAS, 361, 109
Bamford S. P., Milvang-Jensen B., Aragón-Salamanca A., 2007, MNRAS, 378, L6
Bamford S. P., Rojas A. L., Nichol R. C., Miller C. J., Wasserman L., Genovese C. R., Freeman P. E., 2008, MNRAS, 391, 607
Bamford S. P. et al., 2009, MNRAS, 393, 1324
Bamford S. P., Häußler B., Rojas A., Vika M., Cresswell J., 2012, in Tuffs R. J., Popescu C. C., eds, Proc. IAU Symp. Vol. 284, The Spectral Energy Distribution of Galaxies. Cambridge Univ. Press, Cambridge, p. 301
Barnes J. E., Hernquist L. E., 1991, ApJ, 370, L65
Bedregal A. G., Aragón-Salamanca A., Merrifield M. R., 2006, MNRAS, 373, 1125
Bedregal A. G., Cardiel N., Aragón-Salamanca A., Merrifield M. R., 2011, MNRAS, 415, 2063
Bekki K., 2009, MNRAS, 399, 2221
Bekki K., Couch W., Shioya Y., 2002, ApJ, 577, 651
Bekki K., Couch W., Shioya Y., Vazdekis A., 2005, MNRAS, 359, 949
Blake C. et al., 2004, MNRAS, 355, 713
Bösch B. et al., 2013a, A&A, 549, A142
Bösch B. et al., 2013b, A&A, 554, A97
Butcher H., Oemler A., 1978, ApJ, 226, 559
Butcher H., Oemler A., 1984, ApJ, 285, 426
Caldwell N., Rose J., Franx M., Leonardi A., 1996, ApJ, 111, 78
Caldwell N., Rose J., Dendy K., 1999, AJ, 117, 140
Cappellari M., Emsellem E., 2004, PASP, 116, 138
Cardiel N., 2010, indexf: Line-strength Indices in Fully Calibrated FITS Spectra. Astrophysics Source Code Library, ascl:1010.046
Casteels K. R. V. et al., 2013, MNRAS, 429, 1051
Chien L.-H., Barnes J. E., 2010, MNRAS, 407, 43
Christlein D., Zabludoff A. I., 2004, ApJ, 616, 192
Cortesi A. et al., 2013, MNRAS, 432, 1010
Couch W. J., Newell E. B., 1984, ApJS, 56, 143
Couch W., Sharples R., 1987, MNRAS, 229, 423 (CS87)
Couch W., Ellis R., Sharples R., Smail I., 1994, ApJ, 430, 121
Couch W. J., Barger A. J., Smail I., Ellis R. S., Sharples R. M., 1998, ApJ, 497, 188 (C98)
Couch W., Balogh M., Bower R., Smail I., Glazebrook K., Taylor M., 2001, ApJ, 549, 820
Crowl H. H., Kenney J. D. P., 2008, AJ, 136, 1623
Desai V. et al., 2007, ApJ, 660, 1151
Dressler A., 1980, ApJ, 236, 351
Dressler A., Gunn J., 1983, ApJ, 270, 7
Dressler A., Oemler A., Butcher H., Gunn J., 1994, ApJ, 430, 107
Dressler A. et al., 1997, ApJ, 490, 577
Dressler A., Smail I., Poggianti B., Butcher H., Couch W., Ellis R., Oemler A., 1999, ApJ, 122, 51
Driver S. P., Popescu C. C., Tuffs R. J., Liske J., Graham A. W., Allen P. D., de Propris R., 2007, MNRAS, 379, 1022
Eliche-Moral M. C., González-García A. C., Aguerri J. A. L., Gallego J., Zamorano J., Balcells M., Prieto M., 2012, A&A, 547, A48
Eliche-Moral M. C., González-García A. C., Aguerri J. A. L., Gallego J., Zamorano J., Balcells M., Prieto M., 2013, A&A, 552, A67
Elmegreen D. M., Elmegreen B. G., Kaufman M., Sheth K., Struck C., Thomasson M., Brinks E., 2006, ApJ, 642, 158
Fasano G., Poggianti B., Couch W., Bettoni D., Kjaergaard P., Moles M., 2000, ApJ, 542, 673
Fisher D., Franx M., Illingworth G., 1996, ApJ, 459, 110
Font A. S. et al., 2008, MNRAS, 389, 1619
Franx M., 1993, ApJ, 407, L5
Gallazzi A. et al., 2009, ApJ, 690, 1883
Geach J. E., Smail I., Moran S. M., Treu T., Ellis R. S., 2009, ApJ, 691, 783
Goto T., 2003, Ap&SS, 35, 1249
Goto T., 2005, MNRAS, 357, 937
Gunn J., Gott J., 1972, ApJ, 176, 1
Häußler B. et al., 2013, MNRAS, 430, 330

Hopkins P. F. et al., 2009, MNRAS, 397, 802

Izzo C., Kornweibel N., McKay D., Palsa R., Peron M., Taylor M., 2004, The Messenger, 117, 33

Jaffé Y. L. et al., 2011, MNRAS, 417, 1996

Jaffé Y. L., Poggianti B. M., Verheijen M. A. W., Deshev B. Z., van Gorkom J. H., 2012, ApJ, 756, L28

Johnston E. J., Aragón-Salamanca A., Merrifield M. R., Bedregal A. G., 2012, MNRAS, 422, 2590

Johnston E. J., Aragon-Salamanca A., Merrifield M. R., Bedregal A. G., 2013a, preprint (arXiv:1309.2206)

Johnston E. J., Merrifield M. R., Aragón-Salamanca A., Cappellari M., 2013b, MNRAS, 428, 1296

Kauffmann G., White S., Heckman T. M., Menard B., Brinchmann J., Charlot S., Tremonti C., Brinkmann J., 2004, MNRAS, 353, 713

Keel W. C., Kennicutt R. C., Jr, Hummel E., van der Hulst J. M., 1985, AJ, 90, 708

Kennicutt R. C., Jr, Roettiger K. A., Keel W. C., van der Hulst J. M., Hummel E., 1987, AJ, 93, 1011

Koopmann R. A., Kenney J. D. P., 2004a, ApJ, 613, 866

Koopmann R. A., Kenney J. D. P., 2004b, ApJ, 613, 851

Kormendy J., Bender R., 2012, ApJS, 198, 2

Kronberger T., Kapferer W., Ferrari C., Unterguggenberger S., Schindler S., 2008, A&A, 481, 337

Lackner C. N., Gunn J. E., 2012, MNRAS, 421, 2277

Lackner C. N., Gunn J. E., 2013, MNRAS, 428, 2141

Lane K. P., Gray M. E., Aragón-Salamanca A., Wolf C., Meisenheimer K., 2007, MNRAS, 378, 716

Larson R., Tinsley B., Caldwell C., 1980, ApJ, 237, 692

Le Borgne D., Rocca-Volmerange B., Prugniel P., Lanon A., Fioc M., Soubiran C., 2004, A&A, 425, 881

Maltby D. T. et al., 2012, MNRAS, 419, 669

Margoniner V., de Carvalho R., Gal R., Djorgovski S., 2001, ApJ, 548, 143

Masters K. L. et al., 2011, MNRAS, 411, 2026

Masters K. L. et al., 2012, MNRAS, 424, 2180

Mihos J., Hernquist L., 1996, ApJ, 464, 641

Moore B., Katz N., Lake G., Dressler A., Oemler A., 1996, Nature, 379, 613

Moran S. M., Ellis R. S., Treu T., Smith G. P., Rich R. M., Smail I., 2007, ApJ, 671, 1503

Nipoti C., Binney J., 2007, MNRAS, 382, 1481

Norton S., Gebhardt K., Zabludoff A., Zaritsky D., 2001, ApJ, 557, 150

Osterbrock D., 1989, Astrophysics of Gaseous Nebulae and Active Galactic Nuclei. University Science Books, Mill Valley, CA

Pasquini L. et al., 2002, The Messenger, 110, 1

Peng Y.-j. et al., 2010, ApJ, 721, 193

Peng Y.-j., Lilly S. J., Renzini A., Carollo M., 2012, ApJ, 757, 4

Poggianti B. M., Smail I., Dressler A., Couch W. J., Barger A. J., Butcher H., Ellis R. S., Oemler A., Jr, 1999, ApJ, 518, 576

Poggianti B. M. et al., 2009, ApJ, 693, 112

Pracy M., Couch W., Blake C., Bekki K., Harrison C., Colless M., Kuntschner H., de Propris R., 2005, MNRAS, 359, 1421 (P05)

Pracy M., Kuntschner H., Couch W., Blake C., Bekki K., Briggs F., 2009, MNRAS, 396, 1349

Pracy M., Owers M., Couch W., Kuntschner H., Bekki K., Briggs F., Lah P., Zwaan M., 2012, MNRAS, 420, 2232

Pracy M. B. et al., 2013, MNRAS, 432, 3131

Prugniel P., Soubiran C., Koleva M., Le Borgne D., 2007, preprint (astro-ph/0703658)

Rees M. J., Ostriker J. P., 1977, MNRAS, 179, 541

Rose J., Gaba A., Caldwell N., Chaboyer B., 2001, AJ, 121, 793

Rose J. A., Robertson P., Miner J., Levy L., 2010, AJ, 139, 765

Shioya Y., Bekki K., Couch W., De Propris R., 2002, ApJ, 565, 223

Simard L., Mendel J. T., Patton D. R., Ellison S. L., McConnachie A. W., 2011, ApJS, 196, 11

Sparke L. S., Kormendy J., Spinrad H., 1980, ApJ, 235, 755

Swinbank M., Balogh M., Bower R., Zabludoff A., Lucey J., McGee S., Miller C., Nichol R., 2012, MNRAS, 420, 672

Teyssier R., Chapon D., Bournaud F., 2010, ApJ, 720, L149

Tran K., Franx M., Illingworth G., Kelson D., van Dokkum P., 2003, ApJ, 599, 865

Vogt N. P., Haynes M. P., Giovanelli R., Herter T., 2004a, AJ, 127, 3300

Vogt N. P., Haynes M. P., Giovanelli R., Herter T., 2004b, AJ, 127, 3325

Wilman D. J., Oemler A., Jr, Mulchaey J. S., McGee S. L., Balogh M. L., Bower R. G., 2009, ApJ, 692, 298

Wolf C. et al., 2009, MNRAS, 393, 1302

Worthey G., Ottaviani D., 1997, ApJ, 111, 377

Yamauchi C., Yagi M., Goto T., 2008, MNRAS, 390, 383

Yang Y., Zabludoff A. I., Zaritsky D., Mihos J. C., 2008, ApJ, 688, 945

Zabludoff A., Zaritsky D., Lin H., Tucker D., Hashimoto Y., Shectman S., Oemler A., Kirshner R., 1996, ApJ, 466, 104

APPENDIX A: INDIVIDUAL ANALYSIS OF GALAXIES

In this section we include the analysis of each of the galaxies in the sample, with a qualitative description and the figures with individual analysis of each galaxy. This information can be found in the online version.

SUPPORTING INFORMATION

Additional Supporting Information may be found in the online version of this article:

Appendix A. Individual analysis of galaxies (http://mnras.oxford journals.org/lookup/suppl/doi:10.1093/mnras/stt2202/-/DC1).

Please note: Oxford University Press are not responsible for the content or functionality of any supporting materials supplied by the authors. Any queries (other than missing material) should be directed to the corresponding author for the article.

This paper has been typeset from a TeX/LaTeX file prepared by the author.